

## Characterization of the glass transition in vitreous silica by temperature scanning small-angle X-ray scattering

R. BRÜNING<sup>1</sup>(\*), C. LEVELUT<sup>2</sup>, A. FAIVRE<sup>2</sup>, R. LEPARC<sup>2</sup>, J.-P. SIMON<sup>3</sup>, F. BLEY<sup>3</sup>  
and J.-L. HAZEMANN<sup>4</sup>

<sup>1</sup> *Physics Department, Mount Allison University, 67 York Street, Sackville (NB), Canada E4L 1E6*

<sup>2</sup> *Laboratoire des Verres, UMR 5587 CNRS-Université Montpellier II, cc 69, 34095 Montpellier Cedex, France*

<sup>3</sup> *LTPCM-ENSEEG-INPG, UMR-CNRS 5614, B.P. 75, 38042 St. Martin d'Hères Cedex, France*

<sup>4</sup> *Laboratoire de Cristallographie, UPR 5031, CNRS, B.P. 166, 38042 Grenoble, France*

PACS. 64.70.Pf – Glass transition.

PACS. 42.70.Ce – Glasses, quartz.

PACS. 61.10.Eq – X-ray scattering (including small-angle scattering).

**Abstract.** – The temperature dependence of the x-ray scattering in the region below the first sharp diffraction peak was measured for silica glasses with low and high OH content (GE-124 and Corning 7980). Data were obtained upon scanning the temperature at 10, 40 and 80 K/min between 400 K and 1820 K. The measurements resolve, for the first time, the hysteresis between heating and cooling through the glass transition for silica glass, and the data have a better signal to noise ratio than previous light scattering and differential thermal analysis data. For the glass with the higher hydroxyl concentration the glass transition is broader and at a lower temperature. Fits of the data to the Adam-Gibbs-Fulcher equation provide updated kinetic parameters for this very strong glass. The temperature derivative of the observed X-ray scattering matches that of light scattering to within 14%.

*Introduction.* – Although vitreous silica is of great importance for fiber optics communication, technology and science, there has been a relative paucity of data regarding its glass transition. In overviews of the properties of glasses, pure vitreous SiO<sub>2</sub> had to remain a missing data point [1]. Scanning calorimetry is perhaps the most commonly used tool to determine the glass transition temperature,  $T_g$ , and the relaxation state of glasses. For vitreous silica, due to the high  $T_g$ , this method cannot be used without some difficulty, and the first in situ temperature scanning experiment for this material monitored the light scattering [2]. More recently, differential thermal analysis (DTA) measurements have determined the step in the specific heat at the glass transition. An unusual endothermic process takes place during annealing [3], which can be attributed to the diffusion of water/hydroxyl groups [4]. The

---

(\*) E-mail: rbruening@mta.ca

response of vitreous silica to quenching at different rates has been investigated by a molecular dynamics simulation [5]. High temperature small-angle X-ray scattering (SAXS) experiments have been proven as a sensitive method to detect the glass transition, and changes of the state of the glass [6,7]. The relation between thermal analysis methods and temperature scanning SAXS has been established [8], and here we use this method to obtain reference data of high quality for the glass transition in vitreous silica.

*Experimental Method.* – SAXS measurements were carried with the D2AM experimental set-up at the European Synchrotron Radiation Facility (ESRF) at a wavelength of  $\lambda = 0.677 \text{ \AA}$ . Polished plates of GE-124 (six samples) and Corning 7980 (three samples) were measured. The hydroxyl content of the samples was determined with infrared spectroscopy. For the GE-124 samples,  $[\text{OH}] = (2 \pm 1) \text{ wt. ppm}$ , did not change during the experiment. For Corning 7980, the samples in the as-received state contained  $(900 \pm 6) \text{ wt. ppm}$ , and the average  $[\text{OH}]$  decreased to  $(832 \pm 6) \text{ wt. ppm}$  in the course of the measurements. Samples, with dimensions of  $1 \times 4 \times 12 \text{ mm}^3$ , were placed inside a molybdenum furnace equipped with Kapton windows [6, 7, 9]. During the SAXS transmission mode measurements the temperature was scanned at rates of 10, 40 and 80 K/min, while helium near atmospheric pressure flowed through the furnace. The observed melting temperature of a gold foil upon heating at 40 K/min deviated 2 K from the standard value. The heating and cooling curves obtained with the vitreous silica samples are consistent, so that thermal gradients between samples and the thermocouples are negligible. The thermal history of the samples was reset by heating to the top of the temperature range, followed by cooling and heating at the desired rate. For each sample the cool-heat cycle was repeated, typically three times. At the sample surface a small amount of crystallization is visible after the measurements, but no correlation between the SAXS signal and the progress of surface crystallization was found. The SAXS was observed with a fiber optic coupled CCD camera. The acquisition time was 20 s (10 s for 80 K/min scans). Distortions and cosmic tracks in the CCD signal were corrected before integrating it in the azimuthal direction. The x-ray was monitored before the furnace,  $m_0$ , and after the furnace,  $m_1$ , by scattering part of the beam with a Kapton foils onto scintillation counters. Between sample changes the SAXS signal of the empty furnace,  $I^B(q)$ , was measured. Here  $q = 4\pi\lambda^{-1} \sin \theta$  is the scattering vector, and  $\theta$  is half of the scattering angle. This background originated mainly from the Kapton windows and air scattering. Based on the measured signal with the sample in place,  $I^{S+B}(q)$ , the signal originating from the sample was calculated according to

$$I(q) \propto (t \ln 1/t)^{-1} [I^{S+B}(q)/m_1^{S+B} - I^B(q)/m_1^B] m_1^{S+B} / m_0^{S+B}, \quad (1)$$

where the transmission factor  $t = m_1^{S+B} m_0^B / (m_0^{S+B} m_1^B)$  allows for changes in the thickness and orientation of the sample. The scattered intensity was converted to absolute values, in electron units per  $\text{SiO}_2$  composition unit, by scaling the data to the measured signal obtained with water. We assumed the value of 6.37 e.u. per  $\text{H}_2\text{O}$  molecule, which is approximately constant from  $q = 0.3$  to  $0.7 \text{ \AA}^{-1}$  [10]. The probable error of the conversion factor is 4%.

The analysis of the data follows the procedure described in [6]. Fig. 1 shows  $I(q)$ , on a logarithmic scale, as a function of  $q^2$ . Most of the data range corresponds to the low- $q$  tail of the first sharp diffraction peak (FSDP) of vitreous silica [11]. The small structure in the spectrum around  $q^2 = 0.07 \text{ \AA}^{-2}$  is due to residual scattering originating from the Kapton windows. Precision SAXS data show that the SAXS intensity in vitreous silica continues to decrease down to  $q = 0.01 \text{ \AA}^{-1}$  [10,12], so that the rise observed here at low angles is not an inherent property of the material. The linear regime in this plot, extending from  $q^2 \approx 0.04$  to  $0.4 \text{ \AA}^{-2}$ , is well described by  $I(q) = I(0) \exp(bq^2)$ . For each temperature, the parameters  $b$  and  $I(0)$  are obtained by linear regression. The data range included in the regression calculation is

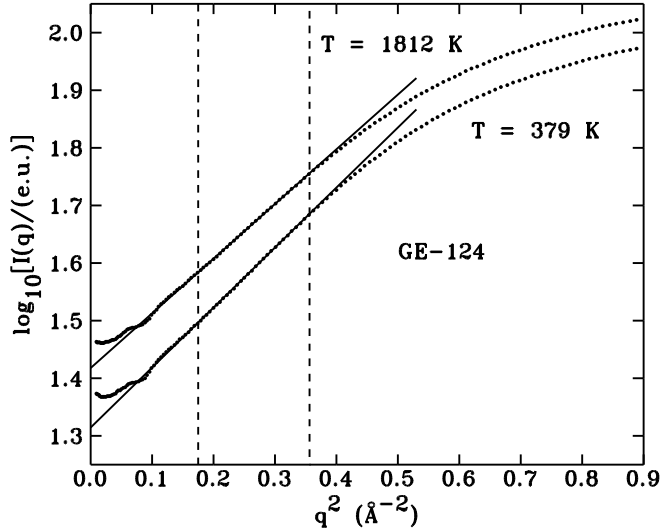


Fig. 1 – Logarithm of the scattered intensity of GE-124 plotted versus  $q^2$  at two temperatures. The solid lines are obtained by linear regression of the data between the dashed vertical lines, and  $I(q = 0)$  is obtained as one of the regression parameters.

indicated by the broken vertical lines in fig. 1. The regression parameters depend only weakly on the range of data.

The extrapolated intensity,  $I(0)$ , rises with increasing temperature, while the slope  $b$  decreases (fig. 1). This temperature dependence is qualitatively similar to results obtained with a fragile glass [8]. For brevity we restrict the discussion to  $I(0)$ , which has lower experimental uncertainty. For GE-124, the overall change of  $I(0)$  is about 20% over the whole temperature range of about 1400 K, fig. 2(a). In the successive temperature scans on the same sample,  $I(0)$  changes slowly by about 2%, and, once upon a refill of the synchrotron,  $I(0)$  increased by 3%. Hence we attribute these effects to changes of the incident beam (e.g. of the energy, the direction or position) which are not fully eliminated by normalizing the signal to the measured X-ray flux before the sample. Linear corrections (less than 2.5%) were applied to the traces shown in fig. 2(a) in order to align the end points of the traces obtained with a given sample.

*Results and Discussion.* – The temperature dependence of the SAXS in fig. 2(a) shows the standard features of the glass transition:  $I(0)$  changes gradually with temperature in the glass state, whereas the supercooled liquid state depends more strongly on temperature. In addition to the change of slope, the glass transition is marked by a hysteresis between the heating and cooling curves. The  $T_g$  of Corning 7890 vitreous silica, with a higher water content, is  $(232 \pm 14)$  K lower than the  $T_g$  of GE-124. Outside the glass transition regime the slopes of the curves are constant. The results of multiple measurements on a given sample, as well as on equivalent samples, agree. A slight difference can be seen in the heating curves for the water-rich sample, which may be caused by the partial loss of water at the sample surface.

The slopes of the straight line segments of the data in fig. 2(a) are given in table I, as well as the corresponding slopes obtained by light scattering [2]. The slopes are normalized to the intensity at an arbitrary temperature above  $T_g$ , where the samples are in metastable equilibrium (1800 K). The light scattering based slopes are higher than the SAXS based results by 11% above  $T_g$ , and 14% below  $T_g$ . Since the data are based on very different ranges of

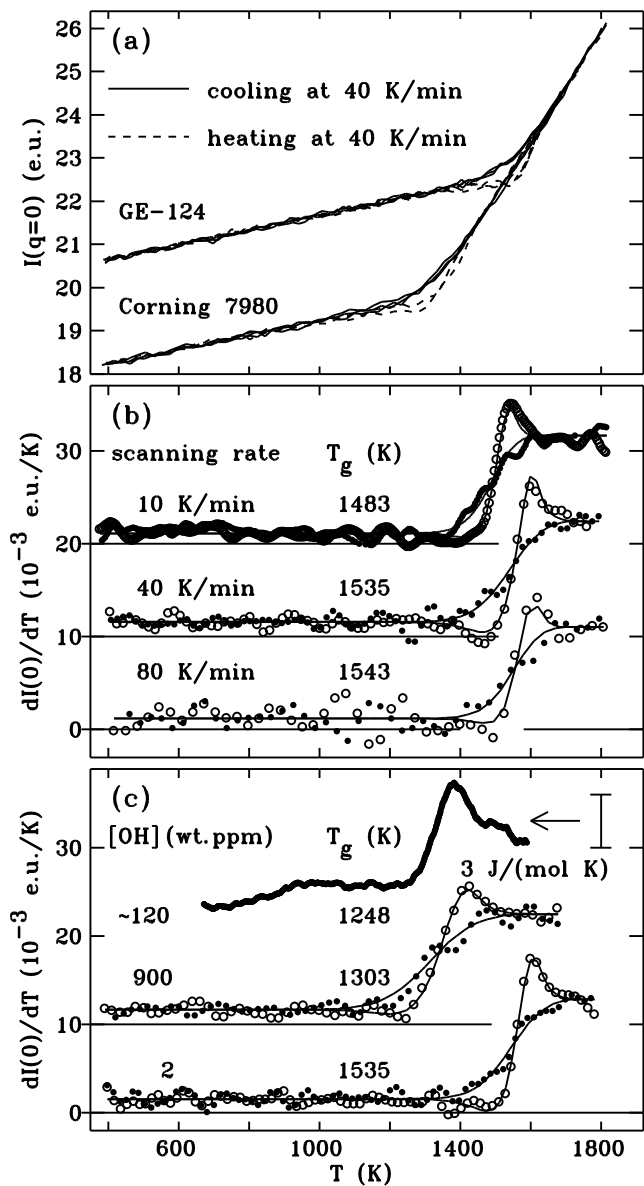


Fig. 2 – (a) Scattered intensity, extrapolated to  $q = 0$ , as a function of temperature. GE-124 contains 2 wt. ppm  $H_2O$ , and Corning 7980 contains 900 wt. ppm  $H_2O$ . (b) Temperature derivatives of  $I(0)$ , obtained for GE-124 upon scanning the temperature at different rates. Full and open symbols show cooling and heating data, respectively. Solid lines are fits to the AGF equation. For clarity, the 40 and 10 K/min curves were shifted up by 10 and  $20 \times 10^{-3}$  e.u./K, respectively. (c) Temperature derivatives of  $I(0)$  data obtained at 40 K/min for GE-124 and, shifted up by  $10 \times 10^{-3}$  e.u./K, Corning 7980. Top: heat flow upon heating a sample with  $\approx 120$  wt. ppm at 40 K/min (ref. [3]).

TABLE I – Comparison of the temperature sensitivity of SAXS and light scattering (last two columns). Normalized temperature derivatives,  $[I(1800\text{ K})]^{-1}dI/dT$ , in units of  $10^{-6}\text{ K}^{-1}$ , are evaluated below and above the glass transition regime. The samples are GE-124, Corning 7980, and, from ref. [2], type A and type G vitreous silica.

[OH] (wt. ppm)	2	900	< 1	1200
$T < T_g$	$74 \pm 2$	$72 \pm 2$	$85 \pm 2$	$85 \pm 3$
$T > T_g$	$500 \pm 6$	$500 \pm 6$	$561 \pm 4$	$561 \pm 4$

photon momentum transfer (extrapolation to  $q = 0$  from the range  $0.2\text{ \AA}^{-1} < q < 0.6\text{ \AA}^{-1}$  for SAXS, and  $q = 1.8 \times 10^{-3}\text{ \AA}^{-1}$  for the light scattering experiment), the approximate agreement of the x-ray and light scattering results is reassuring. It shows that the temperature dependence of density fluctuations is almost wavelength-independent below as well as above  $T_g$ . In one-component materials, the  $q = 0$  limit is related to the compressibility [13]. Low- $q$  scattering in vitreous silica originates predominantly density fluctuations, since the chemical order of the  $\text{SiO}_4$  tetrahedra is nearly perfect [2,6]. Following the analysis of the light scattering data, the slope below  $T_g$  is proportional to the adiabatic compressibility of the glass, and the slope above  $T_g$  is proportional to the isothermal compressibility of the liquid [2,14]. A review of literature data for SAXS and light scattering measurements shows that the compressibilities determined by different methods vary by up to 25% [15].

As a next step we consider the temperature derivative of  $I(0)$ , which provides curves that are comparable to e.g. calorimetric measurements. While linear adjustments were made for the traces in fig. 2(a) (as mentioned above), this was not necessary for fig. 2(b) and (c), since differentiation reduces the effect of the slow drift of  $I(0)$ . High frequencies are enhanced by numeric differentiation. These were partially suppressed by applying a Fourier filter to the differentiated data. The results obtained for GE-124 at three different scanning rates are presented in fig. 2(b). The differentiated curves clearly show the expected hysteresis of the glass state between heating and cooling. The value of  $T_g$  considered here is the low temperature limit of the fictive temperature calculated from the cooling curve of the best fit of the data to the AGF equation (described below). This value is close to the onset of the glass transition, but it has the advantage that it is based on the complete cooling and heating trace. The fitted value of  $T_g$  varies by about 4 K between repeated scans for GE-124, and by 12 K for Corning 7980. The glass transition shifts to higher temperature with increasing scanning rate. A Kissinger plot of  $\ln(\phi T_g^{-2})$  vs.  $T_g^{-1}$ , where  $\phi$  is the temperature scanning rate, yields an activation energy of  $E_a/k_B = (62 \pm 10) \times 10^3\text{ K}$  for GE-124, in agreement with the slope of viscosity data in an Arrhenius plot,  $61.9 \times 10^3\text{ K}$  for a vitreous silica with [OH] < 10 wt. ppm [16].

Fig. 2(c) shows the differentiated data for the GE-124 and Corning 7980 glasses, as well as previously published DTA data obtained for annealed Corning 7980 glass with a reduced hydroxyl content [3]. (In order to demonstrate the degree of reproducibility, the 40 K/min data for Corning 7980 in fig. 2 (b) and (c) are examples from different scans.) A comparison of the SAXS-based curves shows a broader transition for the glass with the higher hydroxyl concentration. This agrees with the slope of the equilibrium viscosity in an Arrhenius plot, which decreases by 28% as the hydroxyl content increases from 3 to 1200 wt. ppm [17]. The increase of the width of the glass transition regime may be caused by the joint action of two processes: At high temperatures direct bond-breaking and relaxation of the  $\text{SiO}_2$  network take place, while below 1100 K the site-to-site diffusion of hydroxyl groups is the faster process [4]. The hydroxyl diffusion process, emergent at low temperatures, can therefore broaden the glass transition curve. The DTA and SAXS based data in fig. 2(c) basically agree, which confirms

the results of the prior series of calorimetric measurements [11]. However, the SAXS data are clearly superior both in terms of the stability and linearity of the background as well as in providing data upon heating as well as cooling. One would expect the glass transition for the 120 wt. ppm sample at a temperature 50 K higher than that of the 900 wt. ppm sample [2].

Next the Adam-Gibbs-Fulcher (AGF) equation is used to extract standard kinetic parameters from the SAXS data. Details beyond the present summary of this approach can be found in [3, 18]. The state of the glass can be approximated by a fictive temperature,  $T_f$ . Above the glass transition,  $T_f$  is equal to the temperature, while upon cooling sufficiently far below the glass transition  $T_f$  becomes frozen with  $T_f = T_g$ . The AGF approximates the relaxation time of the glass and supercooled liquid states as

$$\tau(T, T_f) = A \exp Q/[T(1 - T_0/T_f)], \quad (2)$$

where the temperatures  $Q$  and  $T_0$  are parameters, and  $A$  is the high temperature limit of the relaxation time. This equation extends the Vogel-Fulcher-Tammann equation, to which it reduces in the supercooled liquid regime where  $T_f = T$  [18]. In this case the relaxation time diverges when  $T$  reaches  $T_0$ . The relaxation time is used with the Narayanaswamy-Moynihan equation, which describes how  $T_f$  evolves as

$$T_f(T) = T^* + \int_{T^*}^T \left\{ 1 - \exp \left[ - \left( \int_{T'}^T \frac{dT''}{\phi\tau(T'')} \right)^\beta \right] \right\} dT'. \quad (3)$$

This integral involves a Kohlrausch exponent,  $\beta$ , as a further parameter. Finally, the SAXS data are fitted by treating the temperature derivative of  $I(0)$  far below and far above  $T_g$  as further adjustable parameters. Then we obtain

$$\frac{dI(0)}{dT} = \frac{dI(0)}{dT} \Big|_{T \ll T_g} + \left[ \left( \frac{dI(0)}{dT} \Big|_{T \gg T_g} - \frac{dI(0)}{dT} \Big|_{T \ll T_g} \right) \frac{dT_f}{dT} \right]. \quad (4)$$

The solid lines fig. 2(b),(c) are least-squares fits of the data to the AGF equation. The kinetic parameters of the fits are given in table II.

TABLE II – Parameters of least squares fits to the AGF equation of the SAXS data obtained at 40 K/min for GE-124 and Corning 7980. Experimental errors are estimated from the fit parameter variations for multiple scans obtained with the same sample.

[OH] (wt. ppm)	2	900
$Q$ ( $10^3$ K)	$49 \pm 5$	$39 \pm 9$
$-\lg(A/s)$	$15 \pm 1$	$11 \pm 1$
$T_0$ ( $10^3$ K)	$0.30 \pm 0.16$	$0.05 \pm 0.11$
$\beta$	$0.87 \pm 0.06$	$0.76 \pm 0.05$

For GE-124 ([OH] = 2 wt. ppm), the AGF fit parameters clearly indicate the properties of a very strong glass:  $T_0$  is only 20% of  $T_g$ ,  $\beta$  is close to one as expected [1], and the time prefactor,  $A \sim 10^{-15}$  s, is comparable to the inverse of the Debye frequency. As a comparison, fits to viscosity data give  $Q = 33.53 \times 10^3$  K and  $T_0 = 0.54 \times 10^3$  K [19]. The fit parameters are sensitive to the width and the details of the shape of the glass transition curves. The broader SAXS curve for the high [OH] sample is reflected in the lower  $Q$  and a longer time  $A$ . The change of  $Q$  matches the above-mentioned 28% decrease of the activation energy for the equilibrium viscosities upon increasing [OH] [17]. The new SAXS data provide tighter constraints on the fit as well as a superior signal to noise ratio compared to the DTA data in fig. 2 (c), so that the present fit parameters are more reliable than the values given previously [3].

*Conclusion.* – The present SAXS data provide, for the first time, a clear picture of the glass transition in vitreous silica, including the hysteresis between cooling and heating. The signal to noise ratio is improved over previous point-by-point SAXS, temperature scanning light scattering and DTA measurements. Scanning the temperature at a rate of 40 K/min, has provided the best data. The shift of  $T_g$  with heating rate matches the temperature dependence of the viscosity. Increasing the hydroxyl concentration from 2 to 900 wt. ppm lowers  $T_g$  by  $(232 \pm 14)$  K. The glass with the higher hydroxyl concentration has a broader glass transition, in agreement with the results of non-equilibrium viscosity measurements. The SAXS of vitreous silica is slightly less temperature dependent than the light scattering (11% above and 14% below the glass transition). Based on the present results, the AGF parameters for vitreous silica have been updated.

\* \* \*

We wish to thank O. Geyamond, S. Arnaud, and B. Caillot for technical assistance, as well as J.-F. Bézar for assistance in using beamline BM02. ESRF provided the synchrotron radiation facilities, and the Natural Science and Engineering Research Council of Canada has supported this work through a Discovery Grant.

#### REFERENCES

- [1] BÖHMER R. and ANGELL C. A., (1994) *Disorder Effects on Relaxation Processes* (Springer-Verlag, Berlin, Heidelberg), edited by R. RICHERT AND A. BLUMEN, p. 11.
- [2] SAITO K. and IKUSHIMA A. J., *Appl. Phys. Lett.*, **70** (1997) 3504.
- [3] BRÜNING R., *J. Non-Cryst. Solids*, **330** (2003) 13.
- [4] TOMOZAWA M., (2001) *Silicon-Based Materials and Devices* (Academic Press, NY), edited by H. S. NALWA, p. 127.
- [5] VOLLMAYR K., KOB W. and BINDER K., *Phys. Rev. B*, **54** (1996) 15808.
- [6] LEVELUT C., FAIVRE A., LE PARC R., CHAMPAGNON B., HAZEMANN J.-L., DAVID L., ROCHAS C. and SIMON J.-P., *J. Non-Cryst. Solids*, **307-310** (2002) 426.
- [7] LE PARC R., CHAMPAGNON B., DAVID L., FAIVRE A., LEVELUT C., GUENOT PH., HAZEMANN J.-L., ROCHAS C. AND SIMON J.-P., *Phil. Mag. B*, **82** (2002) 431.
- [8] FAIVRE A., DAVID L., VASSOILLE R., VIGIER G., ETIENNE S. and GEISSLER E., *Macromolecules*, **29** (1996) 8387.
- [9] SOLDI Y., HAZEMANN J.-L., ABDERDAM D., INUI M., TAMURA K., RAOUX D., PERNOT E., JAL J.-F. and DUPUY-PHILON J., *Phys. Rev. B*, **57** (1998) 258.
- [10] LEVELUT A.-M. and GUINIER A., *Bull. Soc. fr. Minéral. Cristallogr.*, **90** (1967) 445.
- [11] BRÜNING R. and COTTRELL D., *J. Non-Cryst. Solids*, **325** (2003) 6.
- [12] RENNINGER A.L. and UHLMANN D.R., *J. Non-Cryst. Solids*, **16** (1974) 325.
- [13] GUINIER A., (1963) *X-Ray Diffraction* (W. H. Freeman and Company), p. 48.
- [14] SCHROEDER, J., MOHR, R., MACEDO P. B. and MONTROSE, C. J., *J. Am. Ceram. Soc.*, **56** (1973) 510.
- [15] WATANABE T., SAITO K. and IKUSHIMA A.J., *J. Appl. Phys.*, **94** (2003) 4824.
- [16] URBAIN G., BOTTINGA Y. and RICHET P., *Geochim. Cosmochim. Acta*, **46** (1982) 1061.
- [17] HETHERINGTON G., JACK K. H. and KENNEDY J. C., *Phys. Chem. Glasses*, **5** (1964) 130.
- [18] HODGE I. M., *J. Non-Cryst. Solids*, **169** (1964) 211.
- [19] SIPP A., BOTTINGA Y. and RICHET P., *J. Non-Cryst. Solids*, **288** (2001) 166.